Electrical properties of ZnO nanorods studied by conductive atomic force microscopy

I. Beinik,[1] M. Kratzer,[1] A. Wachauer,[1] L. Wang,[1] R. T. Lechner,[1] C. Teichert,[1,a)] C. Motz,[2] W. Anwand,[3] G. Brauer,[3] X. Y. Chen,[4] X. Y. Hsu,[4] and A. B. Djurišić[4]
[1]*Institute of Physics, Montanuniversitaet Leoben, Franz-Josef Str. 18, A-8700 Leoben, Franz-Josef Str. 18, A-8700 Leoben, Austria*
[2]*Erich Schmid Institute of Materials Science, Austrian Academy of Sciences, Jahnstrasse 12, A-8700 Leoben, Austria*
[3]*Institut für Strahlenphysik, Helmholtz-Zentrum Dresden-Rossendorf, Postfach 510119, D-01314 Dresden, Germany*
[4]*Department of Physics, University of Hong Kong, Pokfulam Road, Hong Kong, People's Republic of China*

(Received 15 January 2011; accepted 2 May 2011; published online 2 September 2011)

ZnO nanostructures are promising candidates for the development of novel electronic devices due to their unique electrical and optical properties. Here, we present a complementary electrical characterization of individual upright standing and lying ZnO nanorods using conductive atomic force microscopy (C-AFM). Initially, the electrical properties of the arrays of upright standing ZnO NRs were characterized using two-dimensional current maps. The current maps were recorded simultaneously with the topography acquired by contact mode AFM. Further, C-AFM was utilized to determine the local current-voltage (I-V) characteristics of the top and side facets of individual upright standing NRs. Current-voltage characterization revealed a characteristic similar to that of a Schottky diode. Detailed discussion of the electrical properties is based on local I-V curves, as well as on the 2D current maps recorded from specific areas. © *2011 American Institute of Physics*. [doi:10.1063/1.3623764]

I. INTRODUCTION

ZnO nanorod (NR) arrays have been of interest for applications in a variety of optoelectronic devices,[1] including solar cells. For example, ZnO nanowire arrays have been utilized in dye-sensitized solar cells.[2–4] It has been demonstrated that the electron transport in a nanowire array electrode is more efficient compared to a conventional nanoparticle porous film electrode.[2] Thus, the study of electronic properties and charge transport in ZnO nanorod/nanowire arrays is of considerable interest for their practical applications. Consequently, ZnO NRs have been the subject of active studies by means of conductive atomic force microscopy (C-AFM) including experiments with applied mechanical stress.[5–10] This technique is promising for the characterization of as-grown nanostructures and provides the access to electrical properties on the nanoscale.

Although, scanning electron microscopy (SEM) is the method of choice to study arrays of upright standing NRs, also tapping mode AFM has been successfully employed, for instance, to determine height fluctuations in arrays of upright standing NRs and intermediate side facets of the rods.[11]

Here, we present a complementary study of the electrical transport in individual upright standing ZnO NRs utilizing C-AFM. This technique is promising for the characterization of as-grown nanostructures and provides the access to electrical properties on the nanoscale. Applying C-AFM to study the electrical properties of the rods is an additional challenge, since the method operates in contact mode.[12,13] In this technique, a conductive AFM probe is utilized as probing electrode and force sensor at the same time.

The electrical contact area formed between the AFM probe and sample depends on the mechanical properties of the tip's and sample's materials and the tip loading force.[14] Usually, the contact area is ranging from a few square nanometers up to some several hundreds of nanometers, reaching in some cases micrometer size. The size of the contact area determines to a high extent the electrical transport regime.

The electrical transport via the tip-to-sample interface involves usually several mechanisms, such as tunneling, field, and thermal emissions,[15] making an analysis in the majority of cases difficult. Nevertheless, the dual functionality of the conductive probe enables one to influence the electrical transport regime by the application of proper tip loading force thus favoring a certain mechanism of transport.

A poor electric contact stability and ill-defined tip conditions are usually the limiting factors in C-AFM applications. As a solution, a high tip loading force is applied in order to improve the contact stability. The formation and rupture of nanocontacts formed by the conductive AFM tip to ZnO NRs have been a subject of a recent study where it has been shown that a stable electrical contact may be formed with tip loading force as low as $\sim 12\ nN$.[16] Measuring with forces above this value one can expect reproducible behavior of the two-dimensional (2D) current maps and current-voltage (I-V) curves. The I-V characterization of ZnO NRs using C-AFM reveals usually rectifying behavior that can be analyzed in terms of Schottky barrier formation between the C-AFM tip and the NR.[16]

a)Electronic mail: teichert@unileoben.ac.at. URL: http://www.unileoben.ac.at/~spmgroup/.

Here, we applied C-AFM to study electrical properties of as-grown ZnO NRs, which were structurally precharacterized by means of SEM and XRD. C-AFM was used to record 2D current maps simultaneously with topography. These measurements have been complemented by local I-V characterization of the top and side planes of individual NRs. The I-V curves were analyzed using the Shockley diode equation. The electrical and morphological data were correlated.

II. EXPERIMENT

A. Sample preparation

The measurements have been performed on ZnO NRs grown by thermal evaporation of Zn in dry argon flow on fluorine-doped tin oxide (FTO)/quartz substrates. The substrate was placed 1.5 cm above the Zn source (0.2 g, Aldrich, 99.995%). The reaction was performed in a horizontal tube furnace with a base pressure (no gas flow) of $\sim 10^{-2}$ Torr. Prior to growth, the furnace was flushed with 0.1 $L/$ min of argon. When the furnace reached 500 $^{\circ}C$, a flow of 0.01 $L/$ min oxygen gas was added. The pressure during growth was 1.1 Torr, the reaction time was 70 min.[4]

B. Structural characterization

The morphology of the arrays of upright standing ZnO NRs was studied by means of SEM and intermittent contact mode AFM using PPP-NCHR probes from Nanosensors™ with a cantilever resonance frequency of ~330 kHz.

For additional characterization of the ZnO NRs' crystallographic properties as well as their orientation, x-ray diffraction (XRD) measurements were performed. We recorded the XRD-spectra of the ZnO NRs by performing ω-2θ-scans perpendicular to the sample surface using a standard lab diffractometer with an analyzing crystal in front of the detector at 1.54 Å x-ray wavelength.

C. Local electrical characterization

The local electric properties of the NRs have been investigated using an MFP3D™ AFM from Asylum Research equipped with the standard ORCA™ module that allows one to carry out C-AFM experiments and measure currents in the range from 1 pA to 20 nA. Further, a Nanoscope™ IIIa AFM from Digital Instruments equipped with a home built C-AFM module was used, which allows one to measure currents in the range from 50 (fA) to 200 pA.[17]

The investigation of the electrical properties of ZnO NRs has been carried out solely in contact mode AFM. It has been found that the stability of the feedback loop and imaging process in general are strongly dependent on the force constant of the cantilever and the scan rate. The best results for the topography in contact mode were obtained using PPP-EFM ($k = 0.5 - 9.5$ N$/m$) conductive probes, where the feedback loop stability and the image quality are close to those obtained in intermittent contact mode AFM. We also performed C-AFM measurements using DCP11 diamond coated conductive probes from NT-MDT™. Both the topography and current maps recorded with these probes exhibit less stability compared to those obtained using PPP-EFM probes, however, good stability could be achieved when carrying out measurements with deactivated slow scan axis.

Since the roughness of the surface covered with ZnO NRs is very high, several requirements should be fulfilled to make the measurement possible. Relatively stable measurement conditions could be achieved on the NRs with an average diameter of ~600 nm or larger and lengths up to 2.5−3 μm (measured by SEM). Although, the measurements were also performed on smaller ZnO NRs (down to 30 nm in diameter), we did not achieve any reproducible results since the measurements had to be performed in hit-or-miss fashion in order to avoid breaking of the NRs and consequently damaging the tip. This resulted in a large contribution of tunneling/field emission to the observed currents.

It has also been found that instabilities during C-AFM mapping may lead to a wear of the probe's conductive coating. Therefore, the scan velocity during C-AFM mapping was 0.5 μm/s or lower in order to achieve most stable conditions avoiding damages of the tip coating and to minimize the influence of parasitic capacitance effects at the tip-to-sample interface.

The I-V characteristics were recorded between ±10 V applied to the sample at 0.1 Hz of voltage ramping rate and activated feedback loop.

The 2D mapping in C-AFM as well as the tip positioning for I-V characterization have been performed with the scanner driven in a closed-loop mode. We did not observe any significant difference in the stability of the electrical contact for both types of probes at a loading force of ~50 nN.

III. RESULTS

A. Structural peculiarities

Figure 1 summarizes the structural properties of the ZnO NR array. The sample's morphology is presented in the intermittent contact mode AFM image (Fig. 1(a)). We observe NRs with hexagonal cross-section and diameters in the range from 150 to 1200 nm. Along with exactly upright standing NRs, one can find rods that are significantly tilted with respect to the substrate.

The crystallographic orientation of the vertically aligned planes is difficult to define solely from the AFM measurements. However, the tilted side planes are sometimes composed of step bunches separated by (0001) facets that can easily be distinguished from the rest. The height of the steps on the side plane ranges from 22 to 30 nm. The protruding part of the (0001) facet at the steps of the side planes has a width of about 1 − 2 nm.

The difference in the electrical properties between the top and side planes of the ZnO NRs was one of the key issues examined in the present investigation. In order to have an easier access to both the top and side planes, we dealt preferentially with NRs where the side plane is represented by a number of step bunches instead of one crystallographic facet. Such a structure may be also of interest for some practical applications.

In Fig. 1(b) the section of the XRD-spectrum between the $(10\bar{1}0)$ and the $(20\bar{2}2)$ Bragg peak of ZnO is shown as a function of the reciprocal lattice vector q_z along to the

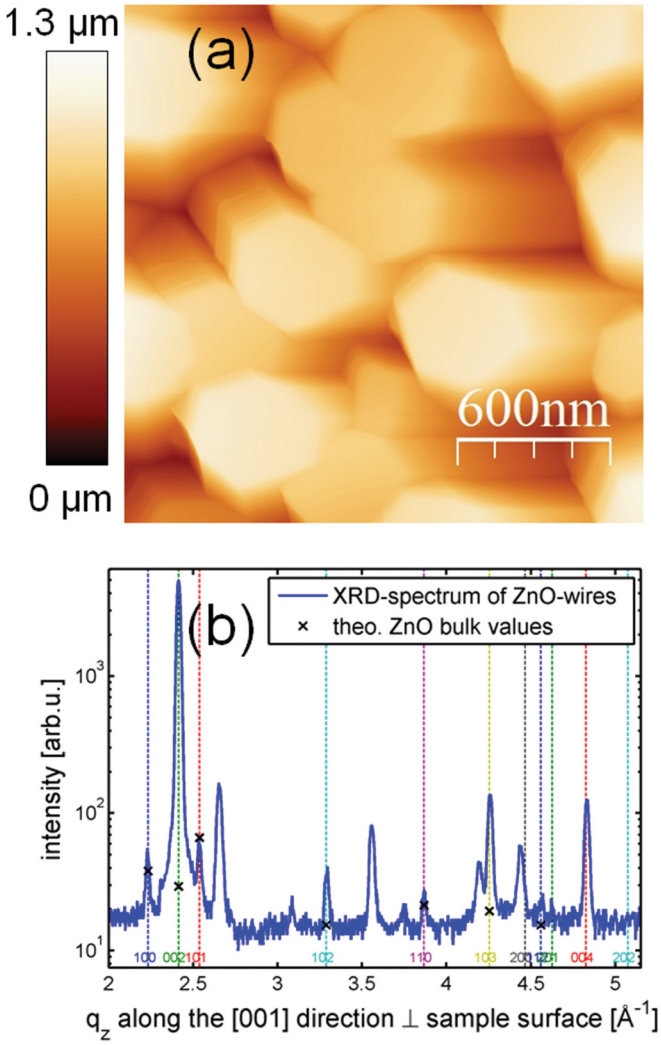

FIG. 1. (Color online) (a) Intermittent contact mode AFM image of ZnO NRs grown on FTO. The diameter of the NRs varied in a wide range from 150 to 1200 nm, the length of the NRs was ~ 2.5 μm as it was determined from the comparison of SEM and AFM data. (b) XRD spectrum of the ZnO NRs perpendicular to the sample surface. XRD intensity over the reciprocal lattice vector q_z along the [0001] direction. ZnO bulk Bragg peak positions and intensities are marked as dashed lines and crosses, respectively.

[0001] direction. The peak positions of bulk wurtzite ZnO with a = 3.250 Å and c = 5.207 Å hexagonal lattice constants are marked by dashed lines and the theoretical peak intensities by crosses. These positions show excellent correspondence to the measured ones proving unstrained crystalline ZnO NRs. (The peaks that have not been indexed can be related to the substrate material.)

Furthermore, we compared the measured integrated peak intensities with the theoretical values for a powder like distribution of ZnO. We found that, e.g., the hexagonal (0002) ZnO peak depicted a 180 times higher intensity as expected for random oriented NRs, related to a majority of ZnO NRs with the c-planes parallel to the sample surface. We could detect only one other preferred lattice plane along the surface normal, i.e., the $(10\bar{1}3)$ plane with ~4 times higher intensity. Assuming a constant volume for all ZnO NRs, we can estimate from all intensity values that 93% of the NRs are aligned with the c-axis along the surface normal. However, 4% are aligned parallel to the $(10\bar{1}3)$ planes of the ZnO NRs, i.e., tilted by 28.1° to the sample surface.

In fact, in our previous AFM study[11] of ZnO NR arrays, we already observed the existence of–in such a way oriented–$\{10\bar{1}3\}$ intermediate facets between the steep $\{10\bar{1}0\}$ side facets and the (0001) top. All other orientation directions are found to contribute below ~1%.

B. 2D current maps

The results of the C-AFM measurements are presented in Fig. 2. Topography images are given in 2D (a) and 3D (b) presentation, respectively, in order to provide a better insight into the structural peculiarities of the investigated system.

The current maps were recorded in forward (from left to right, (a)) and backward (from right to left, (b)) scan directions at sample bias of +0.1 V. The small value of the applied bias is conditioned by the fact that ZnO NRs exhibit a high conductivity, most likely due to their high surface conductivity.[18]

It is seen that the current maps recorded in forward and backward scan direction differ from each other. The current map in the forward direction exhibits more localized and intense current bursts, whereas in the opposite scan the bursts are distributed more homogeneously and have a lower magnitude. The difference is artificial and comes most likely from the non-symmetrical tip geometry with respect to the sample. The appearance of the current bursts, however, is an interesting phenomenon. The current map recorded in the forward scan direction has been post-processed, and the line profiles taken from the post-processed image are subject of further analysis.

The first derivative of the current map is shown in Fig. 3(a). This representation helps to locate the current

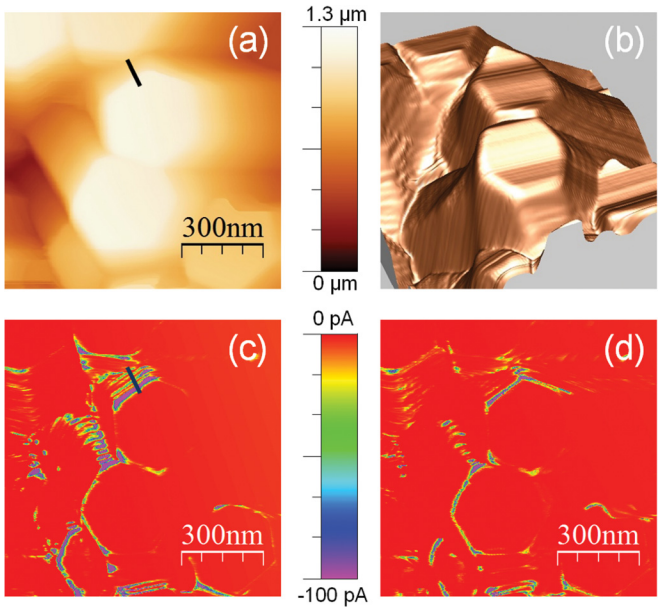

FIG. 2. (Color online) C-AFM images of ZnO NRs grown on FTO. 2D (a) and 3D (b) topography images of ZnO NRs reveal the presence of step bunch-like structures at the side plane instead of a singular facet. The current maps recorded at + 0.1 V of sample bias in forward (c) and backward (d) scan directions demonstrate the presence of current spikes that appear seemingly at the edges within the side plane.

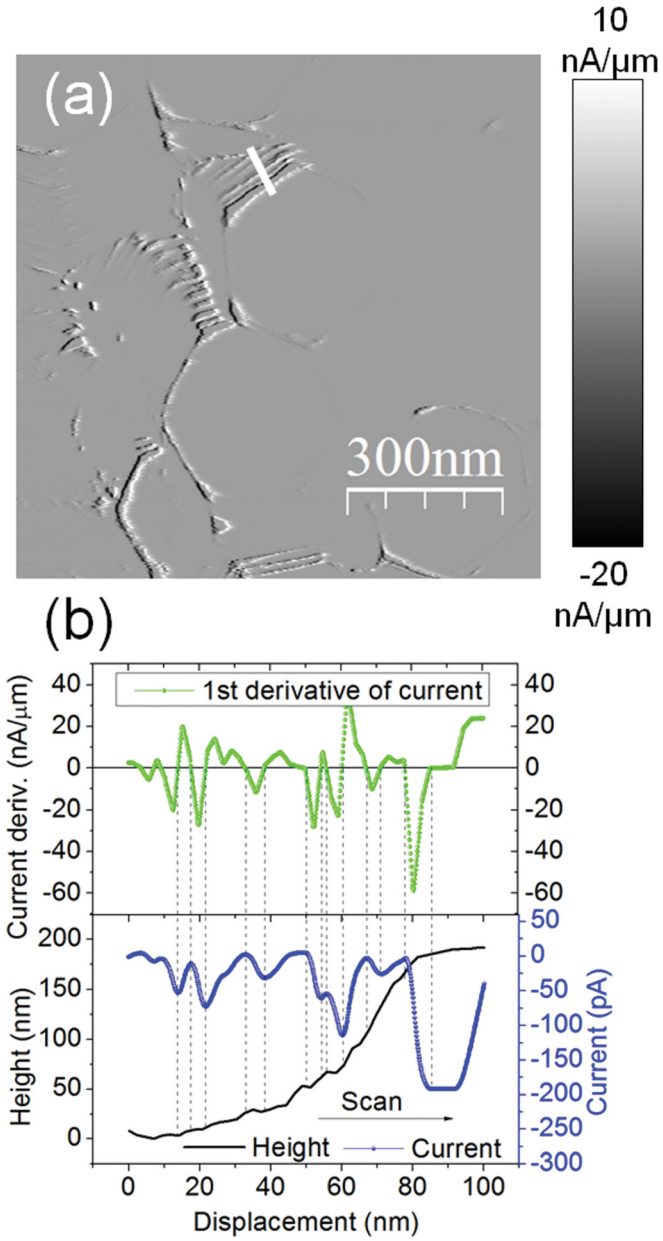

FIG. 3. (Color online) (a) First derivative of the forward current map presented in Fig. 2(c). (b) Correlation between the topography, current, and current derivative profiles taken from the locations marked by correspondently colored lines in Figs. 2(a), 2(c) and Fig. 3(a).

extrema and has been applied in order to perform a simple analysis of the current behavior at the step edges of the side plane of the ZnO NR.

The 2D current map derivative presented in Fig. 3(a) reveals a number of clear bursts coming from the step-like side planes of the ZnO NRs. The points where the current derivative reaches its extrema correspond to the situations when the current changes its behavior from rise to decay or vice versa. The points where the current derivative is equal to zero correspond to either current minimum or maximum.

C. Current line profiles

A comparison of the profiles taken from the current (Fig. 2(c)) and current derivative (Fig. 3(a)) maps with the corresponding topography profile taken from Fig. 2(a), is presented in Fig. 3(b). It provides a clear view into the behavior of the current at the step-like side plane for one of the ZnO NRs. The scan direction is denoted by the arrow in Fig. 3(b). The correlation between zero points on the current derivative profile and corresponding points on the topography is depicted with the help of dashed lines. This kind of behavior is valid for the other NRs inspected, i.e., a general trend is that the current reaches its maximum at the points with a large height gradient, whereas the current minima can be associated with the smaller height gradient.

D. I-V characteristics

The I-V characterization on individual upright standing ZnO NRs has been the subject of our study in order to determine their carrier transport properties. It has been found that for PtIr coated probes, the I-V characteristics are non-reproducible when measuring with tip loading forces of ~50nN or larger. Therefore, the I-V characterization of the ZnO NRs has been performed entirely using diamond coated conductive probes (DCP11 from NT-MDT^{TM}). The low-speed scan direction was turned off at the moment when the NR's position and geometry were defined.

The I-V characteristics presented in Fig. 4 have been recorded at the top and side planes of the ZnO NR with a tip loading force of about 50 nN. Such a loading force is at least twice as large as the one needed to obtain a stable Schottky contact between the PtIr coated tip and ZnO NR.[16] The characteristics reveal that the side plane has a much smaller turn-on voltage that cannot be simply explained via the difference in electrical contact area (see Sec. IV for a detailed discussion).

In fact, the effective electrical contact area has been estimated as 10 nm^2 by a method described by Sarid,[14] and the current densities J used for the presentation in Fig. 4(b) were calculated with this value. The backward diode current (not shown) demonstrated in some cases rather significant deviation from zero level at the sample bias higher than +5.5 V.

We also examined the same structure with diamond coated conductive probes (the data are not presented) and found the same type of electrical behavior, however the electrical contact stability was lower at comparable tip loading forces. Nevertheless, the I-V curves in both cases are asymmetrical, demonstrating rectifying behavior and linearize when presented in an ln$J$ *vs.* V plot (Fig. 4(b)).

IV. DISCUSSION

As mentioned above, C-AFM measurements rely on the fulfillment of several requirements, such as proper tip loading force, scanning rate, applied bias, etc. The 2D current maps measured in contact mode C-AFM revealed a number of current bursts originating from the side planes of the ZnO NRs. The appearance of the current bursts is an interesting phenomena indeed that will be discussed in the following.

At present we assign the difference between backward and forward scan directions of 2D current maps to the non-symmetric tip-to-sample geometry. The current maps in forward and backward directions are recorded with two

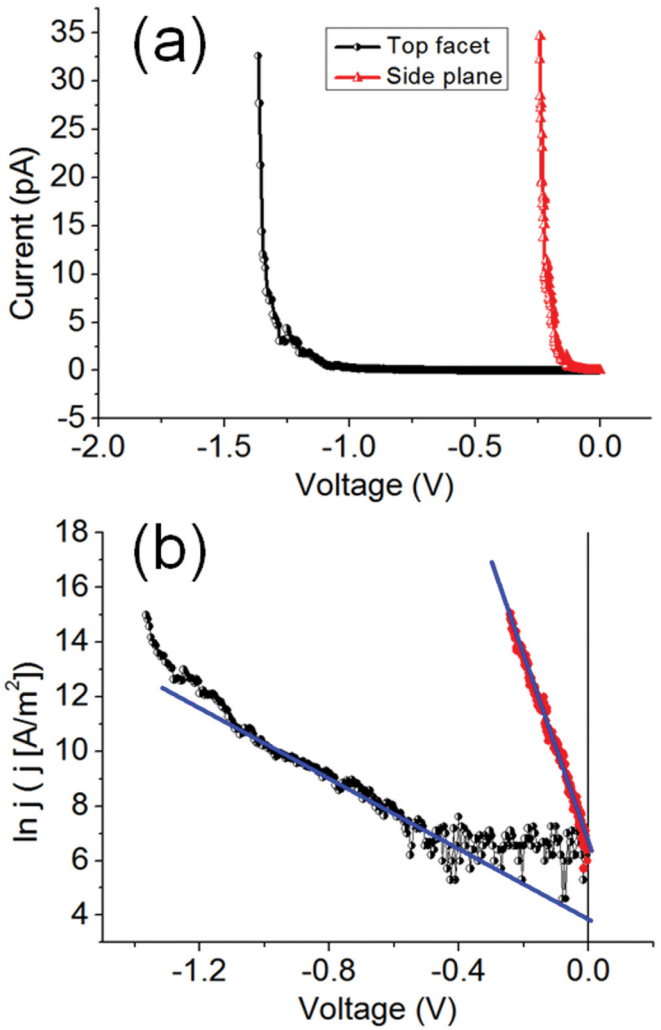

FIG. 4. (Color online) (a) Forward I-V characteristics recorded from the top facet (circles, black) and side plane (triangles, red) of a tilted ZnO NR. The characteristics revealing a significant difference between turn-on voltages. (b) Forward I-V characteristics recorded from the top facet (half-filled circles, black) and side plane (filled circles, red) of a tilted ZnO NR linearized in logarithmic scale. The linear fits (straight lines) were used to determine the Schottky barrier heights and ideality factors.

essentially different electrical contacts (back and front sides of the tip), thus showing some discrepancy.

Several possible mechanisms can be responsible for the appearance of the current bursts. The current bursts appear already at very low sample bias, indicating high conductivity of ZnO NRs and low barrier height between the PtIr coated tip and the ZnO NRs. ZnO is a wide bandgap semiconductor (3.37 eV) (see Ref. 19) and the intrinsic bulk conductivity is very low even if one takes into account that ZnO exhibits n-type conductivity in absence of intentional doping. Studies of the surface conductivity[20–23] reveal that the presence of various adsorbates on the ZnO surface may enhance the conductivity by some orders of magnitude. Also, ZnO exhibits persistent photoconductivity, and its conductive state may persist for very long time like hours or even days.[24,25] Therefore, the pre-exposure to ambient light could also lead to enhanced conductivity.

The analysis of the current derivative profile presented in Fig. 3(b) reveals that the current bursts appear at the points with a large gradient of height. On the first glance, this may serve as an indication for instabilities in the feedback loop of the AFM that cause a rapid increase in the loading force with the consequent decrease of the contact resistance. At the same time, the appearance of the current bursts at the side planes of the NRs may be associated with a larger contact area of the tip-to-sample contact. However, one has to admit that the dependence of the current on the contact area is linear and does not explain the essentially different behavior of the I-V characteristics recorded from the top and side planes (Fig. 4) of the NRs.

We also performed analysis of the I-V characteristics (Fig. 4(b)) in terms of Schottky barrier formation between the tip and the ZnO NR. The values of the Schottky barrier heights have been determined using the diode equation[26]:

$$J = J_0(\exp(-qV_{bias}/\eta k_B T) - 1), \tag{1}$$

where q and k_B are the electron charge and Boltzmann constant, respectively, V_{bias} is the sample bias, T is the temperature, η is the ideality factor, and J_0 is the saturation current density. The I-V characteristics measured from the top and side planes have been linearized in $\ln(J)$ versus V coordinates. The intersection with y-axis gives the value for the saturation current density, which is defined as

$$J_0 = A^{**}T^2 \exp(-q\Phi_{SB}/k_B T), \tag{2}$$

where $A^{**} = 72\ Am^{-2}$ is the Richardson constant for ZnO and Φ_{SB} is the Schottky barrier height (SBH). The saturation current densities determined from the intersection with the y-axis (Fig. 4(b)) equaled to $83.2 \pm 0.1\ Am^{-2}$ and $1077 \pm 0.1\ Am^{-2}$ for the top and side planes, respectively.

The reproducibility of the SBH and corresponding ideality factors for the (0001) top plane for single ZnO NRs was in the range of $\pm 20\%$ for a series of 10 measurements, whereas for the side plane there is no statistics available due to the lack of experimental data caused by technical issues mentioned above. Nevertheless, the estimated value of the SBH for the side plane of ZnO NRs is based on the averaging of reproducible I-V characteristics measured at several locations from different spots on the sample surface. The corresponding SBHs have been estimated as $\sim$0.54 eV and $\sim$0.48 eV for the top and side planes, respectively.

The ideality factors have been determined from the slope of the $\ln(J)$ versus V curves as

$$\eta \equiv \left(\frac{q}{k_B T}\right)\left(\frac{\partial V}{\partial(\ln J)}\right). \tag{3}$$

The ideality factor equaled to $\sim$6.7 for the top and $\sim$1.2 for the side plane, respectively.

We believe that it is worthwhile to collate the ideality factors measured at different voltages for this case, even though they should not be directly compared. A comprehensive overview on SBH for various ZnO crystallographic planes and electrode metals (macroscopic contacts) can be found in the book by Brillson (Ref. 27, p. 486). The SBH for the top facet found in our experiments is smaller than those values found in the literature for the ZnO (0001) top plane,

which already range for this particular plane from 0.61 eV to 0.96 eV (for Pt electrodes). The corresponding ideality factors vary from 1.1 to 3.1.

It is also known that electrical properties of nanocontacts may significantly differ from their microscopic counterparts.[28] In particular, for ZnO Schottky nanocontacts, the values available in the literature are mainly restricted to the ideality factors that range from 3.1 (see Ref. 29) to 9.[30] Since our measurements were carried out under ambient conditions, an influence of hydrogen diffusion originating from electrochemical water decomposition in the contact region can also not be excluded.[31]

According to Allen and Durbin[32] there is not yet a final conclusion concerning the correct model to describe the SBH to ZnO. Furthermore, in contrast to the (0001) plane there are few data available on $(10\bar{1}0)$ side planes.[33] However, from the variation in photoluminescence results of different crystal facets,[34,35] it is reasonable to expect that electrical properties also differ. In addition, secondary ion mass spectroscopy investigation has demonstrated higher incorporation of impurities in O-terminated compared to Zn-terminated ZnO epitaxial films.[36] Moreover, different facets may exhibit differences in surface adsorption (for example, it was proposed that the (0001) surface has affinity to OH groups while the $(000\bar{1})$ surface exhibits affinity to H atoms), which would affect their optical and electronic properties.[37]

Since the ideality factor of the Schottky contact formed between the side plane of the ZnO NR and conductive PtIr probe is close to unity in our case, thermionic emission can be considered as the main mechanism of transport. The electrical transport is driven by the drift of charge carriers due to the electric field applied, rather than due to the non-thermal generation-recombination processes that can take place at the tip-to-sample interface or in the depletion region. For the contact between the top plane and the probe, the deviation of the ideality factor from unity could be caused by several reasons. A high rate of non-equilibrium generation-recombination processes is considered commonly as a main mechanism causing deviation of the ideality factor from unity. Other important influences are the shunt, series resistances, image-force lowering effects, and tunneling.

The analysis of 2D current maps and I-V characteristics recorded with different types of conductive probes (using the same tip loading force) reveal a difference in the magnitudes of the current recorded. Comparison of the current maps recorded with PtIr (PPP-EFM from Nanosensors^{TM}) and conductive diamond coated probes (DCP11 from NT-MDT^{TM}) reveals that the utilization of the latter leads usually to smaller current magnitudes. This is most likely due to the increased barrier height between the tip and ZnO NRs. The second important parameter defining the magnitude of the current flowing via the tip-to-sample interface is the contact resistance that can be regulated to some extent by the force applied to the tip.

V. CONCLUSIONS AND OUTLOOK

In this work we investigated the electrical properties of as-grown ZnO NRs by means of C-AFM. The 2D current maps have been recorded solely in contact mode using PtIr coated probes. The current maps revealed current bursts at the side planes of the NRs and a discrepancy between the scans recorded in backward and forward directions. We assign this discrepancy to be most probably due to the asymmetrical tip geometry, whereas the observed current bursts originate from the difference in the electrical properties between the side and top planes of the ZnO NRs. However, we cannot rule out completely that they appear as a result of instabilities in the feedback loop as reported recently.[8]

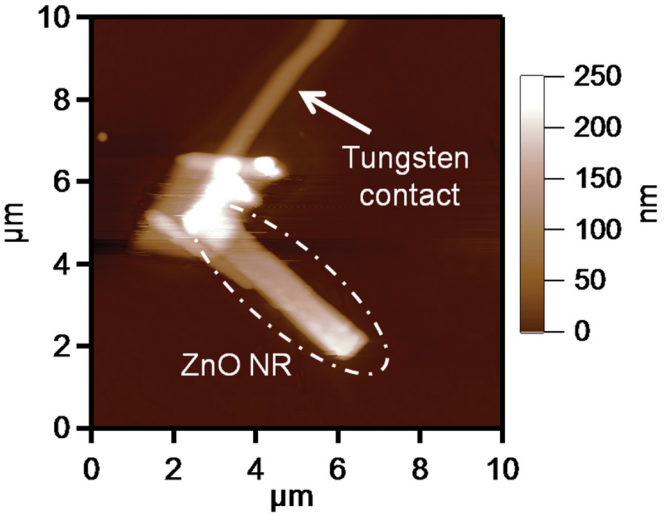

FIG. 5. (Color online) Topography of a ZnO NR lying on an insulating substrate (native oxide covered silicon wafer) and contacted with tungsten by focused ion beam. This setup is planned to be use for C-AFM inspection of the NR side facets.

In order to gain more clarity about the correlation between the structural peculiarities and electrical properties, we performed preliminary C-AFM experiments on lying ZnO NRs, which are presented in Fig. 5. For this experiment, the ZnO NRs prepared by the method described above were mechanically removed from the substrate, dispersed by an organic solvent on an insulating substrate and contacted with tungsten by the help of focused ion beam lithography. We expect that the C-AFM experiments performed in this configuration will help to rule out the artifacts. With C-AFM measurements we faced so far problems resulting from contamination of the NRs with residuals of the organic solvent used. However, we expect that experiments performed in this configuration will help to rule out the possible artifacts mentioned.

For I-V characterization of upright standing NRs, we used diamond coated, conductive probes. These measurements revealed Schottky barrier heights equal to ~0.54 eV and ~0.48 eV for the top and side planes, respectively. Thus, the lower Schottky barrier height for the contact to the side plane of the ZnO NR also contributes to higher currents. Therefore, this difference of the Schottky barrier heights for the side and top planes of the ZnO NRs should be taken into account when analyzing the appearance of the 2D current bursts. The other influences like parasitic capacitance effects, leakage currents, etc., cannot be completely excluded from the consideration.

In this study, we were limited to ZnO NRs with diameters of 600 nm and larger since C-AFM is performed in

contact mode. Smaller NRs were found to not withstand the high lateral forces required. In principle, embedding of NRs in a polymer matrix[9] could solve this problem. However, the resulting functionalization is expected to alter their electrical properties. Finally, we would like to mention that stability problems during C-AFM measurements in air, which are most probably due to the presence of adsorbates, are expected to be circumvent by future measurements using our C-AFM set-up operating under UHV conditions,[38] which has already been successfully applied to study high-k dielectric thin films[39] and lying semiconductor nanowires.[40]

ACKNOWLEDGMENTS

This work was financially supported by the Austrian Science Fund (FWF) under Project No. P19636-N20 and No. P18942-N20. We also acknowledge the help of J. Keckes and M. Bartosik from ESI-Leoben.

[1]A. B. Djurišić, A. M. C. Ng, and X. Y. Chen, Prog. Quantum Elect. **34**, 191 (2010).
[2]M. Law, L. E. Greene, J. C. Johnson, R. Saykally, and P. D. Yang, Nature Mater. **4**, 455 (2005).
[3]E. Galoppini, J. Rochford, H. H. Chen, G. Saraf, Y. C. Lu, A. Hagfeldt, and G. Boschloo, J. Phys. Chem. B **110**, 16159 (2006).
[4]Y. F. Hsu, Y. Y. Xi, A. B. Djurišić, and W. K. Chan, Appl. Phys. Lett. **92**, 133507 (2008).
[5]Z. L. Wang, Mater. Sci. Eng. R: Rep. **64**, 33 (2009).
[6]K. Cheng, G. Cheng, S. J. Wang, L. S. Li, S. X. Dai, X. T. Zhang, B. S. Zou, and Z. L. Du, New J. Phys. **9**, 214 (2007).
[7]Z. L. Wang and J. Song, Science **312**, 242 (2006).
[8]M. Alexe, S. Senz, M. A. Schubert, D. Hesse, and U. Gösele, Adv. Mater. **20**, 4021 (2008).
[9]D. A. Scrymgeour and J. W. P. Hsu, Nano Lett. **8**, 2204 (2008).
[10]W. Guo, Y. Yang, J. Liu, and Y. Zhang, Phys. Chem. Chem. Phys. **12**, 14868 (2010).
[11]G. Brauer, W. Anwand, D. Grambole, W. Skorupa, Y. Hou, A. Andreev, C. Teichert, K. H. Tam, and A. B. Djurišić, Nanotechnol. **18**, 195301 (2007).
[12]G. Brauer, W. Anwand, D. Grambole, W. Egger, P. Sperr, I. Beinik, L. Wang, C. Teichert, J. Kuriplach, J. Lang, S. Zviagin, E. Cizmar, C. C. Ling, Y. F. Hsu, Y. Y. Xi, X. Y. Chen, A. B. Djurišić, and W. Skorupa, Phys. Status Solidi C **6**, 2556 (2009).
[13]C. Teichert and I. Beinik, in *Scanning Probe Microscopy in Nanoscience and Nanotechnology*, edited by B. Bhushan (Springer, Berlin, 2011), Vol. **2**, pp. 691–721.
[14]D. Sarid, *Exploring Scanning Probe Microscopy with Mathematica* (Wiley-VCH, Berlin, 2007).
[15]Y. Sun, H. Mortensen, S. Schär, AS. Lucier, Y. Miyahara, P. Grütter, and W. Hofer, Phys. Rev. B **71**, 193407 (2005).
[16]B. Pérez-García, J. Zúñiga-Pérez, V. Muñoz-Sanjosé, J. Colchero, and E. Palacios-Lidón, Nano Lett. **7**, 1505 (2007).
[17]S. Kremmer, S. Peissi, C. Teichert, and F. Kuchar, in *ISTFA 2002. Proceedings of the 28th International Symposium for Testing and Failure Analysis* (ASM International, Materials Park, 2002), pp. 473–82.
[18]H. J. Krusemeyer, Phys. Rev. **114**, 655 (1959).
[19]C. Klingshirn, Phys. Status Solidi B **244**, 3027 (2007).
[20]J. Aranovich, J. Vac. Sci. Technol. **16**, 994 (1979).
[21]G. Sberveglieri, Sens. Actuators B **23**, 103 (1995).
[22]S. J. Pearton, D. P. Norton, K. Ip, Y. W. Heo, and T. Steiner, J. Vac. Sci. Technol. B **22**, 932 (2004).
[23]O. Schmidt, A. Geis, P. Kiesel, C. G. V. de Walle, N. M. Johnson, A. Bakin, A. Waag, and G. H. Döhler, Superlattices Microstruct. **39**, 8 (2006).
[24]R. Collins, Phys. Rev. **112**, 388 (1958).
[25]I. Beinik, M. Kratzer, A. Wachauer, L. Wang, C. Teichert, Yu. P. Piryatinski, G. Brauer, X. Y. Chen, and A. B. Djurišić, "Photo-response from single upright standing ZnO nanorods," unpublished.
[26]S. M. Sze and K. K. Ng, *Physics of Semiconductor Devices* (John Wiley and Sons, Hoboken, 2007).
[27]L. J. Brillson, *Surfaces and Interfaces of Electronic Materials* (Wiley-IEEE, Weinheim, 2010).
[28]G. D. J. Smit, S. Rogge, and T. M. Klapwijk, Appl. Phys. Lett. **81**, 3852 (2002).
[29]Z. Z. Shao, L. Y. Wen, D. M. Wu, X. A. Zhang, S. L. Chang, and S. Q. Qin, Phys. E **43**, 173 (2010).
[30]W. I. Park, G. Yi, J. Kim, and S. Park, Appl. Phys. Lett. **82**, 4358 (2003).
[31]Y. Dong, Z. Q. Fang, D. C. Look, G. Cantwell, J. Zhang, J. J. Song, and L. J. Brillson, Appl. Phys. Lett. **93**, 072111 (2008).
[32]M. W. Allen and S. M. Durbin, Phys. Rev. B **82**, 165310 (2010).
[33]U. Grossner, S. Gabrielsen, T. M. Borseth, J. Grillenberger, A. Y. Kuznetsov, and B. G. Svensson, AIP Conf. Proc. **772**, 181 (2005).
[34]R. E. Sherriff, D. C. Reynolds, D. C. Look, B. Jogai, J. E. Hoelscher, T. C. Collins, G. Cantwell, and W. C. Harsch, J. Appl. Phys. **88**, 3454 (2000).
[35]H. Sasaki, H. Kato, F. Izumida, H. Endo, K. Maeda, M. Ikeda, Y. Kashiwaba, I. Niikura, and Y. Kashiwaba, Phys. Status Solidi C **3**, 1034 (2006).
[36]S. Lautenschlaeger, J. Sann, N. Volbers, B. K. Meyer, A. Hoffmann, U. Haboeck, and M. R. Wagner, Phys. Rev. B **77**, 144108 (2008).
[37]D. C. Oh, T. Kato, H. Goto, S. H. Park, T. Hanada, T. Yao, and J. J. Kim, Appl. Phys. Lett. **93**, 241907 (2008).
[38]S. Kremmer, C. Teichert, E. Pischler, H. Gold, F. Kuchar, and M. Schatzmayr, Surf. Interface Anal. **33**, 168 (2002).
[39]S. Kremmer, H. Wurmbauer, C. Teichert, G. Tallarida, S. Spiga, C. Wiemer, and M. Fanciulli, J. Appl. Phys. **97**, 074315 (2005).
[40]P. Tejedor, L. Díez-Merino, I. Beinik, and C. Teichert, Appl. Phys. Lett. **95**, 123103 (2009).